# Equilibrium Design of a Wheeled Vehicle for Measuring the Outer Diameter of Straight Stainless Steel Pipes

Guanglei Wu, Yulong Liu, Wenjie Yang, Ziyang Ma, and Bin Niu

**Abstract** This work presents the integrated design of a straight moving vehicle for measuring outer diameter of circular tube. Differing from the current climbing robots or wheeled-mechanisms based on permanent magnet, the motion stability of the designed vehicle is realized by the moment equilibrium, in which the equilibrium condition, interpreting relationship between the moment caused by the mass of vehicle and the friction forces, is derived. A physical prototype is developed and experimental tests verify the equilibrium design approach.

G. Wu
State Key Laboratory of High-performance Precision Manufacturing, School of Mechanical Engineering, Dalian University of Technology, Dalian 116024, China
e-mail: gwu@dlut.edu.cn

Y. Liu
State Key Laboratory of High-performance Precision Manufacturing, School of Mechanical Engineering, Dalian University of Technology, Dalian 116024, China

W. Yang
State Key Laboratory of High-performance Precision Manufacturing, School of Mechanical Engineering, Dalian University of Technology, Dalian 116024, China

Z. Ma
State Key Laboratory of High-performance Precision Manufacturing, School of Mechanical Engineering, Dalian University of Technology, Dalian 116024, China

B. Niu
State Key Laboratory of High-performance Precision Manufacturing, School of Mechanical Engineering, Dalian University of Technology, Dalian 116024, China

## 1 Introduction

Large-length (i.e., max. 100 m) circular seamless tubes are usually used in heavy industry, for instance, the pipelines in ship equipment [10]. Commonly, a heat-forging seamless tube has a nominal outer diameter during its production, and identification of exact dimensions of outer diameter at different cross sections are essential in many applications. High-precision measurement accuracy of the circular tube can be realized by making use of the commercial devices designated for diameter measurement, whereas, the prices of such kind of devices are usually very high, particularly, it is unaffordable for many small and medium enterprises (SMEs). Instead, numerous SMEs adopt calipers to measure the diameter manually, resulting in low efficiency and operator fatigue. In this light, low-cost, high-accuracy and high-adaptability measurement devices are required in previously mentioned industrial sector.

So far, a number of in-pipe robots have been developed [6], which are inapplicable for detection of outer diameters. Aiming at detection of external surfaces or outer wall of pipelines, a common approach is to design the inspection robots based upon the magnet, wherein the magnetic force is generated to keep the robot adhesive to the detected objects. For instance, a marine vessel inspection robot was developed to inspect the surface of ship hull [3]. Such robots, a.k.a., wall-climbing robots, can move on the inclined and vertical convex surfaces [2, 5]. Therefore, permanent magnetic wheeled-mechanisms or climbing robots have been developed to inspect the quality of outer walls of pipelines [1, 7, 8]. It is noteworthy that most of the inspection robots are applicable to the pipelines with relatively large diameters (i.e., $\Phi D \geq 300\,\text{mm}$). Another critical issue should be noted that the reported robots will fail in detecting the stainless steel pipes due to the nonexistence of magnetic force. The other common design approach is to make the climbing robot envelope the tube with articulated linkages [4], whereas, it is difficult to make the long tube as a simply supported beam with avoidance of mechanical collisions. In addition, integrating the inertial measurement unit (IMU) and pose adjusting mechanisms to the robot can improve the self-balancing capability [11], whereas, it will introduce difficulties to the workers due to the complex control strategy.

This work presents the integrated design of a low-cost and high-reliability vehicle to measure the outer diameter of circular tubes, of which the design requirements are listed as below:

- Lightweight: the total mass of the integrated vehicle is less than 2.5 kg;
- High measurement accuracy: the measured error is less than 0.05 mm;
- High stability: the vehicle should move without losing balance;
- High adaptability: one vehicle is applicable to measure multiple tubes with simple structure (i.e., diameter $\Phi D \in [40, 90]\,\text{mm}$, length $l \in [10, 100]\,\text{m}$);
- Soft contact: surface scuffing does not occur after vehicle moves.

Accordingly, the focus lies in the equilibrium design due to the lateral offset of center of mass (CoM) of the integrated vehicle from the neutral axis of the tube, in order to prevent the vehicle from falling down. The equilibrium condition is derived by means of load distributions of steady state vehicle and moment equilibrium, and based on which, an approach to realize the equilibrium is formed. Finally, a prototype of the integrated vehicle that is able to measure a series of different cross-section tubes is built, which is experimentally validated.

## 2 Mechanical Structure of the Vehicle

With the foregoing design requirements, the conceptual design of the vehicle is to meet:

- the vehicle moves along the tube with four wheels for steady motion;
- additional rollers are designed with more contacts to envelope the tube;
- a pair of rollers with large height are designed to detect the out diameter for different tubes, and elastic contacts between the rollers and tube surface are adopted to adapt the varying diameter;
- rollers are selected with soft material (preferably rube) to generate large frictions without surface scuffing.

Accordingly, the CAD model is shown in Fig. 1, with front axle driving and passive rear axle. Eight contact positions are symmetrically distributed around the tube by the the rolling wheels and passive rollers to constrain the straight movement of the vehicle and to generate friction for resistance to the unbalanced moment caused by the CoM offset. Two rear bearing rollers are adopted to detect the tube diameter, which can also produce friction forces. The contacts between the passive rollers and the tube surface are constrained by spring pretensions, adaptive to detect the outer walls of tubes with different and varying diameters.

## 3 Equilibrium Analysis of Steady State Vehicle

Considering that the vehicle moves along the tube without high speed, the moment equilibrium around the tube axis is key to the steady motion of the vehicle. Figure 2 depicts the force diagram of the steady state vehicle on the tube with radius $R$ and downhill angle $\phi$, and $F_x$ represents the rolling resistance force to make the vehicle move forward with constant velocity, and $\mu_i$, $i = 1, 2, 3$, denotes the friction coefficients of different contact areas. The remaining symbols will be interpreted after the following derived equations.

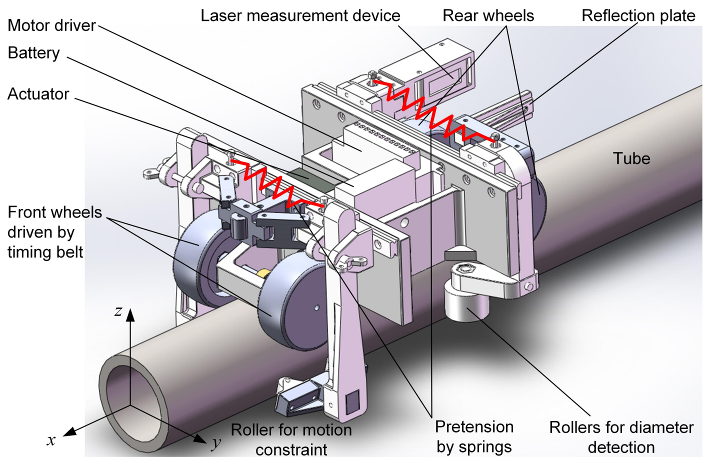


**Fig. 1** CAD model of the wheeled vehicle.

From the force diagram as shown in Fig. 2(a), the equilibrium equations concerning the load on front and rear axles along the longitudinal direction can be used to calculate the distribution of the tyre loads [9]. Henceforth, the moment equilibrium around rear contact between the wheels and tube can be derived, namely,

$$mg(L_r \cos\phi + h \sin\phi) - F_{zf}(L_f + L_r) = 0 \quad \Rightarrow \quad F_{zf} = mg\frac{L_r \cos\phi + h \sin\phi}{L_f + L_r} \tag{1}$$

where $m$ stands for total mass of the vehicle, and $g = 9.805$ represents the vertical acceleration. Moreover, $F_{zf}$ depicts the tyre load on the front axle, and $L_f$, $L_r$ stand for the horizontal distances between the vehicle CoM and the front and rear axles, respectively, together with the perpendicular distance $h$ of the vehicle CoM to the contact line between tyre and tube.

By the same toke, moment equilibrium around front contact and the tyre load $F_{zr}$ on the rear axle are expressed as

$$F_{zr}(L_f + L_r) - mg(L_f \cos\phi - h \sin\phi) = 0 \quad \Rightarrow \quad F_{zr} = mg\frac{L_f \cos\phi - h \sin\phi}{L_f + L_r} \tag{2}$$

Sequentially, the normal tire loads of the front and rear wheels on left- and right-hand sides are given by

$$F_{zf}^L = F_{zf}\frac{R\sin\alpha + r_y}{2R\sin\alpha},\ F_{zf}^R = F_{zf}\frac{R\sin\alpha - r_y}{2R\sin\alpha} \tag{3}$$

$$F_{zr}^L = F_{zr}\frac{R\sin\alpha + r_y}{2R\sin\alpha},\ F_{zr}^R = F_{zr}\frac{R\sin\alpha - r_y}{2R\sin\alpha} \tag{4}$$

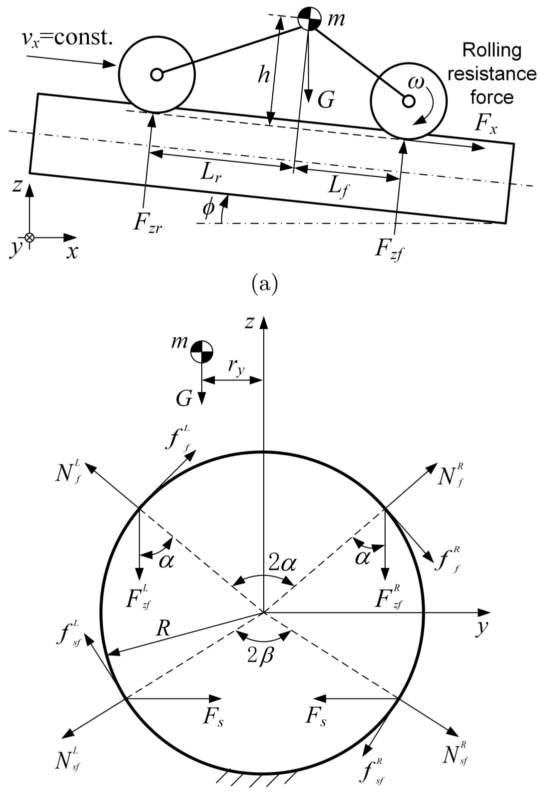


**Fig. 2** Force diagram in longitudinal direction (a) and front axle in lateral direction (b) for the steady state vehicle in equilibrium configuration.

To enable the vehicle can move along the tube steadily, the equilibrium in the lateral direction is to be analyzed. The first step is to find the moment around the neutral axis of the tube generated by the vehicle CoM, calculated as

$$M_G = mgr_y \tag{5}$$

where $r_g$ represents the offset of vehicle CoM parallel to $y$-axis from $xz$ plane.

On the other hand, the moment $M_f^L$ by the friction force $f_f^L$ of the left tyre on the front axle is calculated as below

$$M_f^L = f_f^L R = \mu_1 N_f^L R = \mu_1 F_{zf}^L R \cos\alpha \tag{6}$$

where $\mu_1$ represents the friction coefficient of the contact between the tyre and tube, and $N_f^L$ depicts the normal load, and $2\alpha$ is the central angle with respect to (w.r.t.) chord length determined by the contact points of the two front wheels. Similarly, the moment $M_f^R$ by the friction force $f_f^R$ of the right tyre on the front axle is calculated as

$$M_f^R = f_f^R R = \mu_1 N_f^R R = \mu_1 F_{zf}^R R \cos\alpha \tag{7}$$

By the same token, the moments $M_r^L$ and $M_r^R$ related to the tyre loads on the rear axle can be derived as following

$$M_r^L = \mu_1 F_{zr}^L R \cos\alpha,\ M_r^R = \mu_1 F_{zr}^R R \cos\alpha \tag{8}$$

Let us suppose that $F_s$ represents the pulling force by the spring pretension, the moments generated by the friction forces of the rollers on the front axle are expressed as

$$M_{sf}^L = f_{sf}^L R = \mu_2 N_{sf}^L R = \mu_2 F_s R \sin\beta \tag{9a}$$

$$M_{sf}^R = f_{sf}^R R = \mu_2 N_{sf}^R R = \mu_2 F_s R \sin\beta \tag{9b}$$

where $F_s = k_s(\delta_f - \delta_0)$, and $k_s$, $\delta_f$, $\delta_0$ represent the spring constant, elongation and neutral length of the linear spring. Similarly, the moments by the friction forces of the rollers on the rear axle are calculated as

$$M_{sr}^L = M_{sr}^R = \mu_3 F_s' R,\ F_s' = k_s(\delta_s - \delta_0) \tag{10}$$

In accordance with the load distributions of the tyres and rollers, the moment to resist the moment by the CoM offset equals to the following summation

$$\begin{aligned} M_f &= M_f^L + M_f^R + M_r^L + M_r^R + M_{sf}^L + M_{sf}^R + M_{sr}^L + M_{sr}^R \\ &= \frac{2\mu_1 mgRL_r \cos\phi\cos\alpha}{L_f + L_r} + 2\mu_2 F_s R \sin\beta + 2\mu_3 F_s' R \end{aligned} \tag{11}$$

To this end, the equilibrium condition, represented in terms of the mass–radius product, to make the vehicle run along the circular tube is found as

$$M_G \le M_f \quad \Rightarrow \quad mr_y \le 2R\left(\mu_1 \cos\phi\cos\alpha \frac{mL_r}{L_f + L_r} + \mu_2 \sin\beta \frac{F_s}{g} + \mu_3 \frac{F_s'}{g}\right) \tag{12}$$

If the mass property of the constructed vehicle prototype cannot meet the Eq. (12), a simple approach to realize the moment equilibrium in Eq. (12) is to add a counter mass $m_c$ to the opposite direction of the offset $r_y$ with distance $r_c$. In this view, the new $y$–axis coordinate $r_y'$ of vehicle CoM turns to

$$r_y' = \frac{mr_y - m_c r_c}{m + m_c} \tag{13}$$

## 4 Integrated Design and Test of the Vehicle

Figure 3 shows a prototype of the integrated vehicle, of which the vehicle body frame and major components are fabricated with 3D printing technology for lightweight design. The vehicle is actuated with a set of $42^{\#}$ step motor outputting continuous torque 0.4 Nm with driver TBS6600. A set of two pulleys and one timing belt are adopted to connect the motor shaft and front axle of the vehicle to provide the actuation. A laser measurement device with the measurement range $50 \pm 15$ mm, repeated accuracy 0.03 mm and linear accuracy $\pm 0.1\% F.S.$ is selected. Moreover, the corresponding communication frame is shown, wherein an ESP–32 BLE/Wifi module is adopted as the microcontroller unit (MCU) in order to equip a wireless vehicle for long distance measurement and RS-485 is used as the communication protocol among different modules.

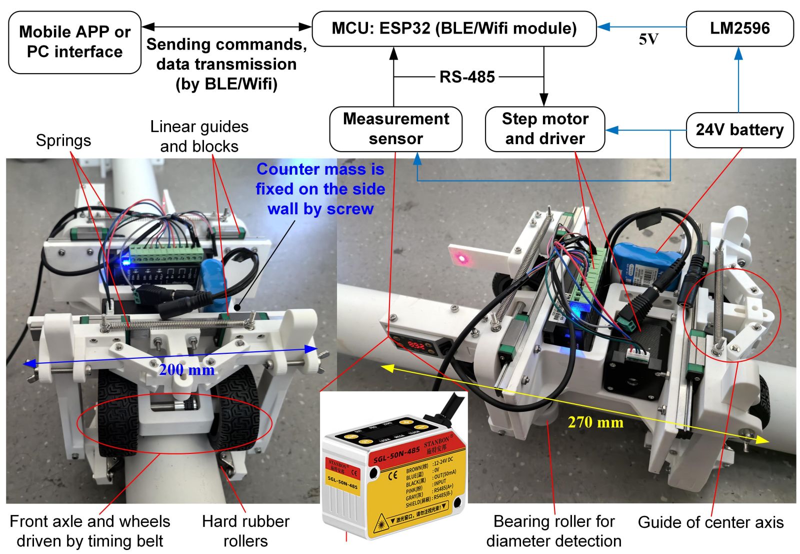


**Fig. 3** An integrated design of vehicle with its communication frame.

The positions of the 3D-printed components CoMs can be found by making use of CAD model after defining material PLA, and the vehicle CoM can be determined by integrating the commercial components. In Fig. 3 for experimental test, the vehicle is placed on a tube made up of PVC with radius 35 mm, and it is applicable to measure the tubes with radii $R \in [64, 80]$ mm without mechanical collision between the bottom surface of the vehicle frame and the tube top. In this design, the structural parameters (unit in length: mm) and mass properties (unit: kg) of the whole vehicle are experimentally verified as listed in Table 1. Besides, the spring constant and neutral length are $k_s = 0.5\,\text{N/mm}$ and $\delta_0 = 80\,\text{mm}$.

**Table 1** Structural parameters and mass properties of the integrated vehicle design.

| $m$ | $L_f$ | $L_r$ | $r_y$ | $h$ | $\phi$ | $\alpha$ | $\beta$ | $(\mu_1,\,\mu_2,\,\mu_3)$ | $(\delta_f,\,\delta_r)$ |
|---|---|---|---|---|---|---|---|---|---|
| 1.336 | 53.05 | 112.40 | 7.8 | 53.5 | 5° | 59.60° | 73.96° | (0.1, 0.07, 0.03) | (93.1, 101) |

Substituting the parameters into Eq. (12) leads to

$$M_G = 101.88\,\text{Nmm},\ M_f = 84.86\,\text{Nmm} \tag{14}$$

which shows that the current design cannot ensure the whole vehicle move along the tube steadily. In light of the moment equilibrium, a counter mass is to be added opposite to $r_y$. Aiming to enhance the adaptability, namely, measurement of multiple tubes with different radii, and considering the lateral dimensions of the vehicle frame, the design space of the mass–product of the added counterweight should be subject to the following limits of structural parameters, i.e.,

$$\begin{cases} \alpha = 66.3°,\ \beta = 76.4°,\ h = 52.7,\ \delta_f = 88.0,\ \delta_r = 95:\ R = 32 \\ \alpha = 48.8°,\ \beta = 76.5°,\ h = 53.4,\ \delta_f = 103.6,\ \delta_r = 111:\ R = 40 \end{cases} \tag{15}$$

from which one can obtain

$$m_c r_c \in [3.75,\ 5]\,\text{kg}\cdot\text{mm},\ \begin{cases} m_c = 0.75 \quad \text{if} \quad r_c = 5 \\ m_c = 0.1 \quad \text{if} \quad r_c = 50 \end{cases} \tag{16}$$

For lightweight design, a counter mass $m_c = 0.093\,\text{kg}$ is selected to add to the vertical wall of the vehicle body on the side with battery installed. Multiple experimental tests, with different moving speeds, are carried out to examine the reliability of the developed vehicle until it falls down from the tube, and a simple spirit level is used for horizontal calibration of the vehicle. The corresponding results are given in Table 2, which turns out that the vehicle can move steadily along the tube for a long distance, i.e., validation of the equilibrium design approach of the built vehicle prototype. On the other hand, structural design is to be improved for longer moving distance.

**Table 2** Experimental test results of the vehicle.

| | $v_x = 0.523\,\text{m/s}$ | | | | | $v_x = 1.047\,\text{m/s}$ | | | | | measure |
|---|---|---|---|---|---|---|---|---|---|---|---|
| test no. | 1 | 2 | 3 | 4 | 5 | 1 | 2 | 3 | 4 | 5 | accuracy |
| distance [m] | 61 | 33 | 45 | 52 | 38 | 54 | 73 | 35 | 65 | 47 | 0.01–0.04 mm |

## 5 Conclusions

Aiming at measurement of outer diameter of circular stainless steel pipes, a lightweight, low-cost and high-adaptability vehicle moving along outer wall of straight tube is developed in this work. Apart from the reported climbing robots or wheeled-mechanisms based on permanent magnet in the literature, the relationship between the moment around the tube axis caused by the mass of vehicle and the friction forces is derived for equilibrium design, based on the load distributions of steady state vehicle and moment equilibrium. The approach to add counter mass is adopted to balance the vehicle in the lateral direction, and a prototype of the wireless vehicle is developed. Experimental tests validates the equilibrium design approach and application potentials.

**Acknowledgements** The reported work was supported by National Natural Science Foundation of China (Grant No.52575268) and the Fundamental Research Funds for the Central Universities (DUTZD25104)

## References

1. Ali, H., Batai, S., Akynov, A.: Vision-based robot for boiler tube inspection, pp. 475–482. Springer International Publishing, Cham (2020)
2. Briones, L., Bustamante, P., Serna, M.: Wall-climbing robot for inspection in nuclear power plants. In: Proc. 1994 IEEE Int. Conf. Robot. Autom., pp. 1409–1414. San Diego, CA, USA (1994)
3. Eich, M., Vögele, T.: Design and control of a lightweight magnetic climbing robot for vessel inspection. In: 2011 19th Mediterranean Conf. Control Autom. (MED), pp. 1200–1205. Corfu, Greece (2011)
4. Gao, G., Du, X., Feng, Y., Wang, S., Wang, F., Zhang, Z.: Mechanical structure design and analysis of the outside needle pipe climbing robot. Adv. Mech. Eng. **14**, 168781402110,310 (2022)
5. Hu, J., Han, X., Tao, Y., Feng, S.: A magnetic crawler wall-climbing robot with capacity of high payload on the convex surface. Robot. Auto. Syst. **148**, 103,907 (2022)
6. Kahnamouei, J.T., Moallem, M.: A comprehensive review of in-pipe robots. Ocean Eng. **277**, 114,260 (2023)
7. Li, H., Hou, Y., Jiang, Y., Sun, W.: Structural design and mechanical analysis of permanent magnet wheeled climbing robots on an outer wall of pipelines. J. Mech. Trans. **47**, 48–54 (2023)
8. Lu, X., Guo, D., Chen, Y.: Design and optimization of the magnetic adsorption mechanism of a pipeline-climbing robot. J. Mech. Sci. Technol. **35**, 5161–5171 (2021)
9. Rajamani, R.: Vehicle Dynamics and Control, chap. Longitudinal Vehicle Dynamics, pp. 87–111. Springer US, Boston, MA (2012)
10. Wei, Z., Wu, J., Li, Z., Cheng, S., Yan, X., Wang, S.: The intelligent layout of the ship piping system based on the optimization algorithm. Appl. Sci. **14**, 2694 (2024)
11. Zhang, H., Mohamad Nor, N.: Control strategies for two-wheeled self-balancing robotic systems: a comprehensive review. Robotics **14**, 101 (2025)